Supporting Information

In-situ synthesis of CNTs@Ti_3C_2 hybrid structures by microwave irradiation for high-performance anodes in lithium ion batteries

W. Zheng[1], P.G. Zhang[1], J. Chen[11], W.B. Tian[1], Y.M. Zhang[2], Z.M. Sun[12]

1 Jiangsu Key Laboratory of Advanced Metallic Materials, School of Materials Science and Engineering, Southeast University, Nanjing 211189, China

2 Jiangsu Key Laboratory of Construction Materials, School of Materials Science and Engineering, Southeast University, Nanjing 211189, PR China

[1] Corresponding author. Tel. +86 025-52090688; E-mail address: j.chen@seu.edu.cn

[2] Corresponding author. Tel. +86 025-52091086; E-mail address: zmsun@seu.edu.cn

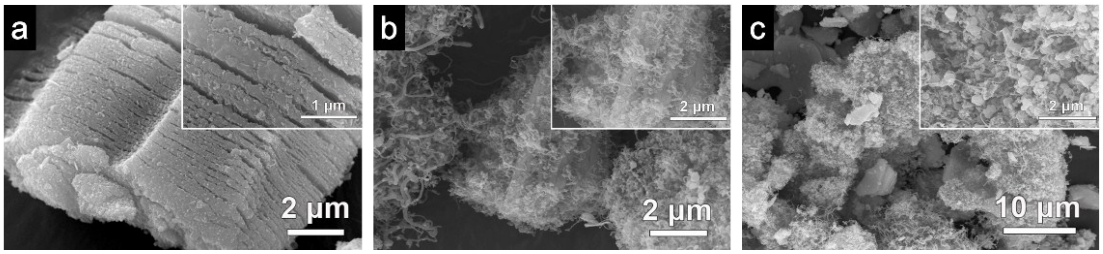

Figure S1. SEM images of CNTs@Ti_3C_2- Ⅰ with different microwave irradiation time: (a) 20 seconds; (b) 40 seconds; (c) 60 seconds.

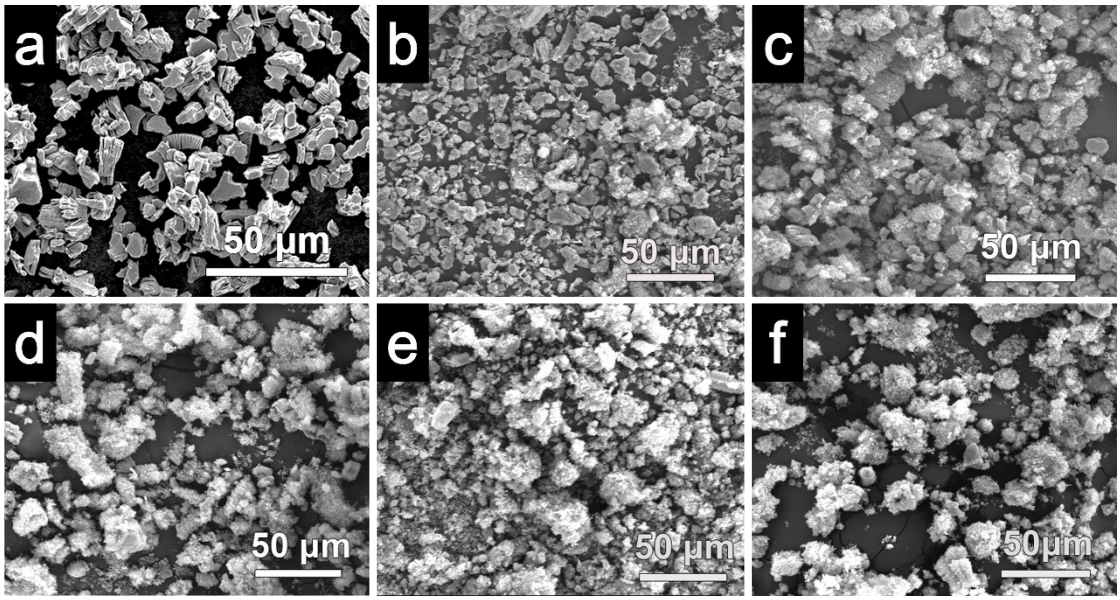

Figure S2. SEM images of (a) Ti_3C_2; (b) CNTs@Ti_3C_2-Ⅰ; (c) CNTs@Ti_3C_2-Ⅱ; (d) CNTs@Ti_3C_2-Ⅲ; (e) CNTs@Ti_3C_2-Ⅳ and (f) CNTs@Ti_3C_2-Ⅴ.

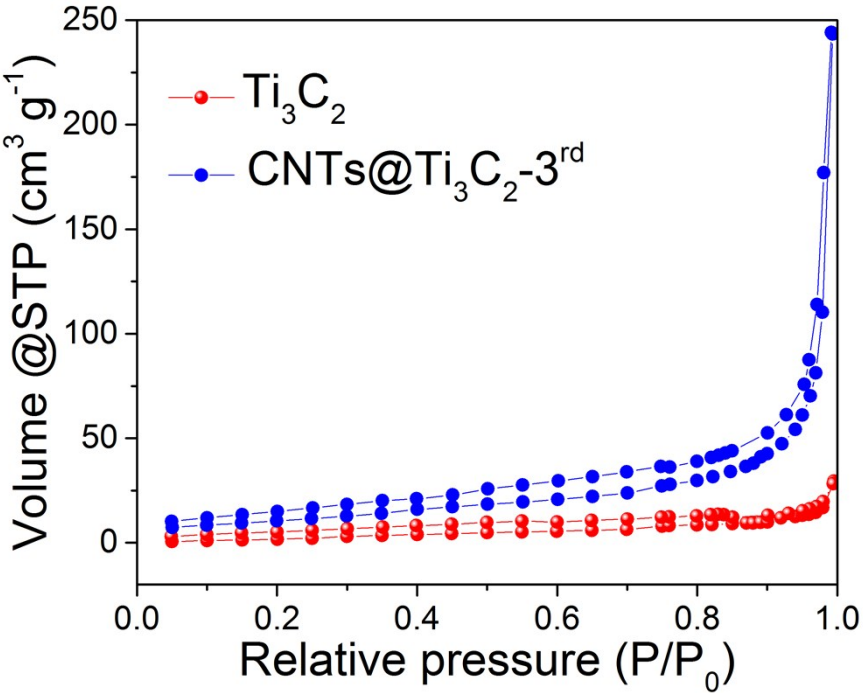

Figure S3. Nitrogen adsorption and desorption isotherms of Ti_3C_2 and CNTs@Ti_3C_2-Ⅲ.

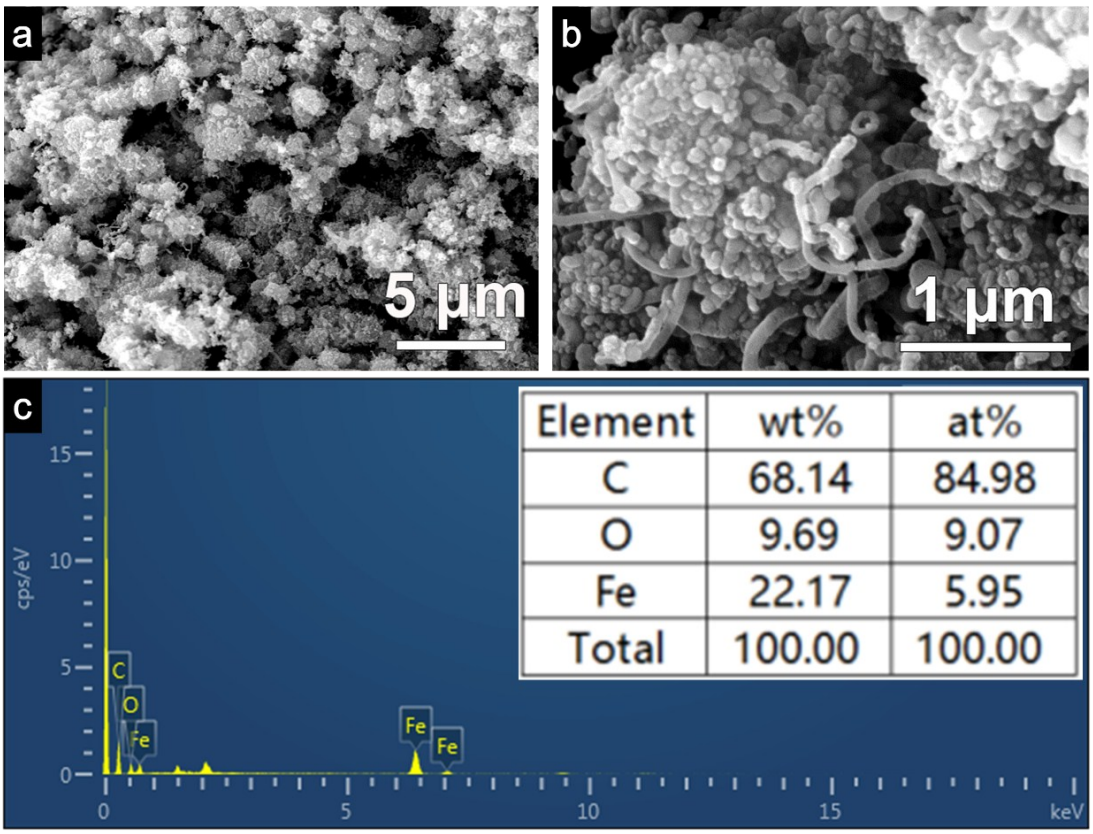

Figure S4. (a)-(b) SEM image of C/CNTs-Ⅰ. (c) the typical EDS. Inset of (c) shows the content of C, O and Fe elements averaged with 6 data in 20*20 μm of square. Carbon nanoparticles and CNTs can be observed clearly in (a) and (b).

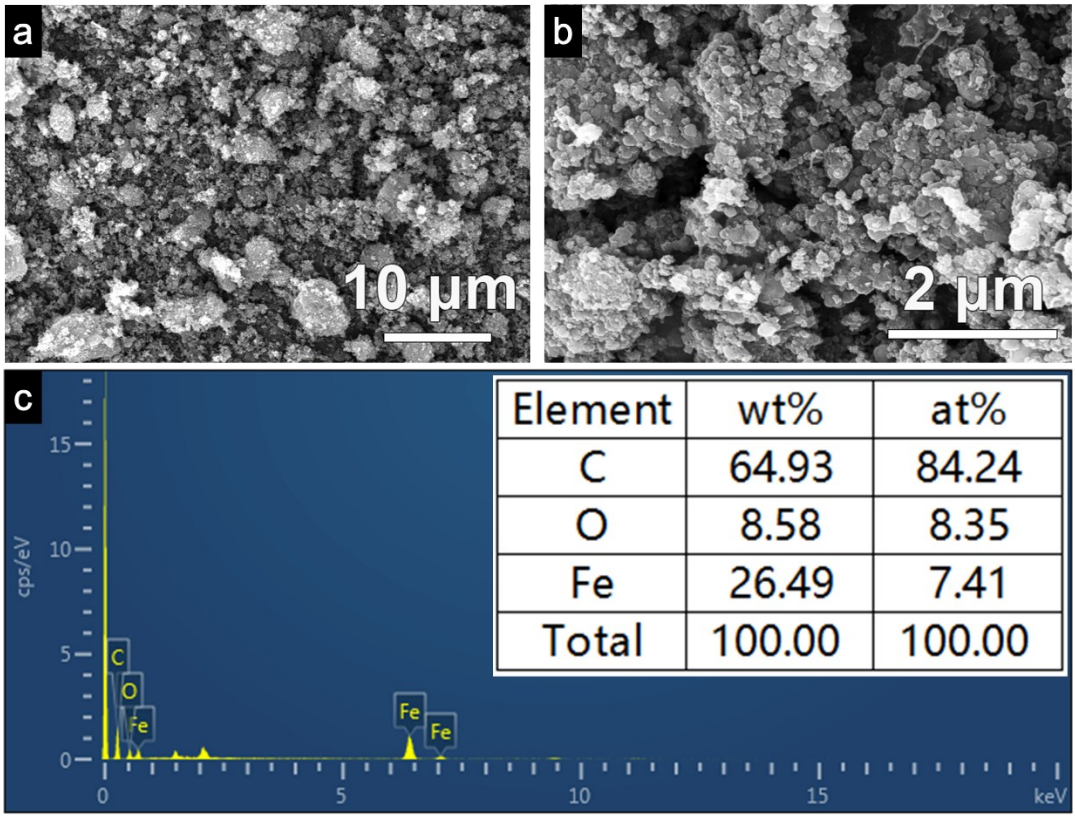

Element	wt%	at%
C	64.93	84.24
O	8.58	8.35
Fe	26.49	7.41
Total	100.00	100.00

Figure S5. (a)-(b) SEM image of C/CNTs-Ⅲ. (c) the typical EDS. Inset of (c) shows the content of C, O and Fe elements averaged with 6 data in 20*20 μm of square. Few CNTs can be observed in (a) and (b).

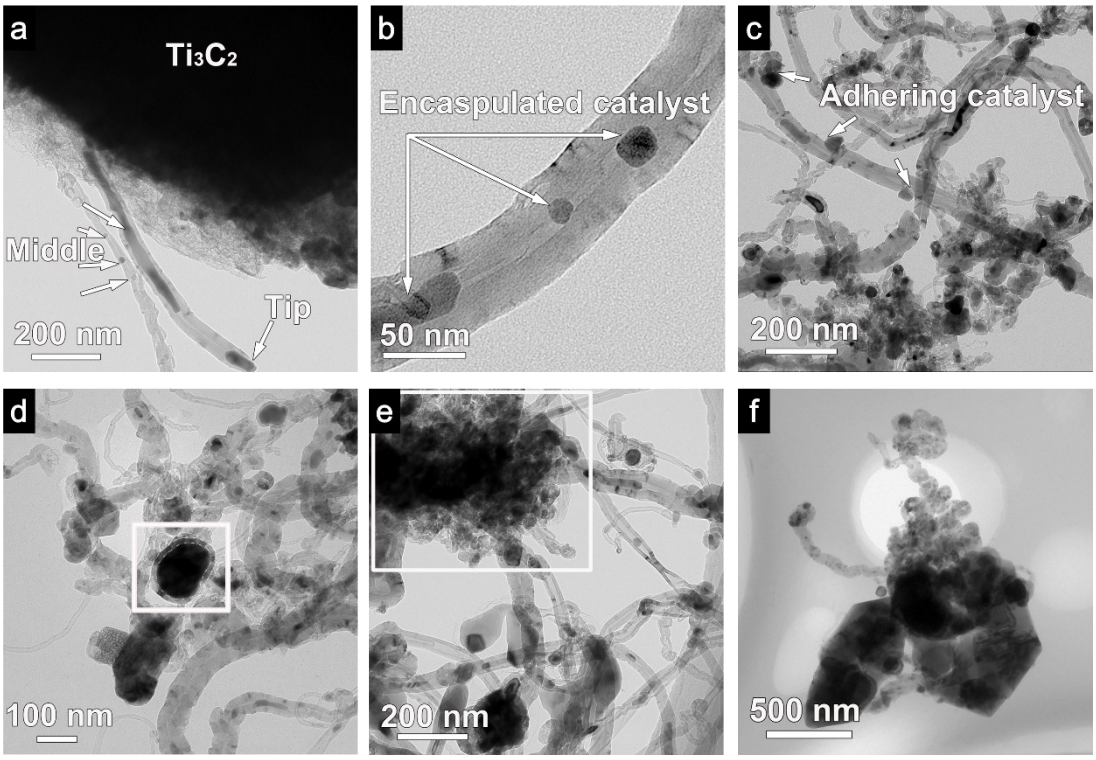

Figure S6. TEM images of CNTs: (a) Catalyst particles encapsulated at the tip or in the middle of the CNTs; (b) Catalyst particles encapsulated inside of the CNTs; (c) Catalyst particles adhering on the surface of the CNTs. (d) One catalyst particle coated by carbon layer (in square); (e) CNTs and carbon particles on metal oxides cluster (in square); (f) Curly CNTs growing from catalyst.

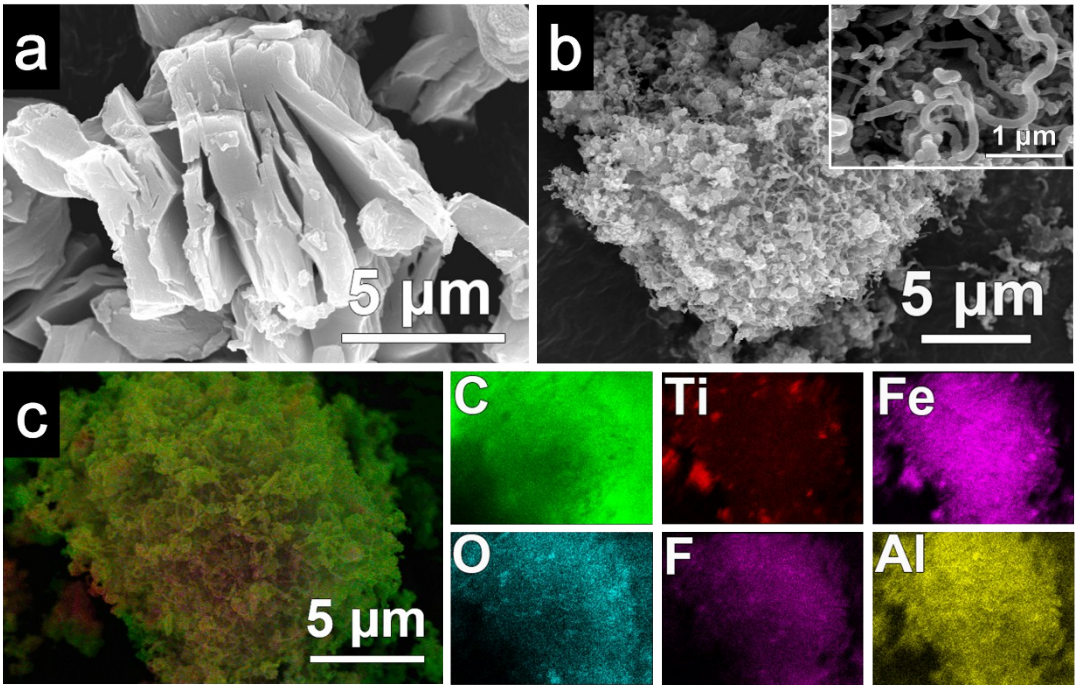

Figure S7. SEM micrographs of (a) Ti_2C; (b) CNTs@Ti_2C; (c) The elements distribution mapping of CNTs@Ti_2C; Inset of (b) shows the amplification of CNTs@Ti_2C.

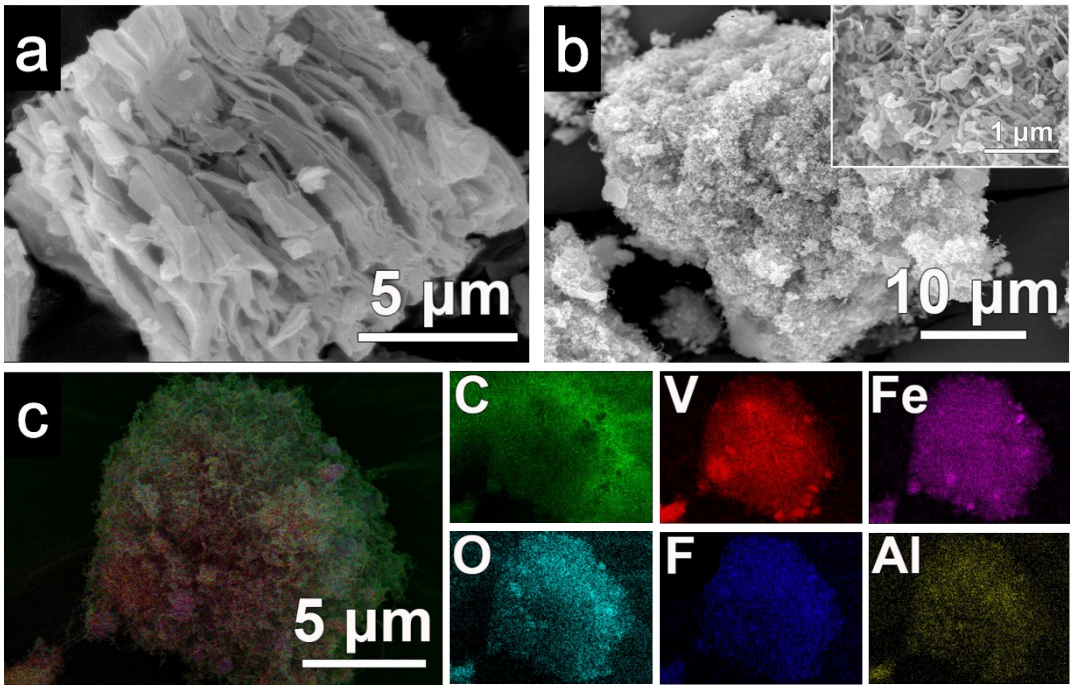

Figure S8. SEM micrographs of (a) V_2C; (b) CNTs@V_2C; (c) The elements distribution mapping of CNTs@V_2C; Inset of (b) shows the amplification of CNTs@V_2C.

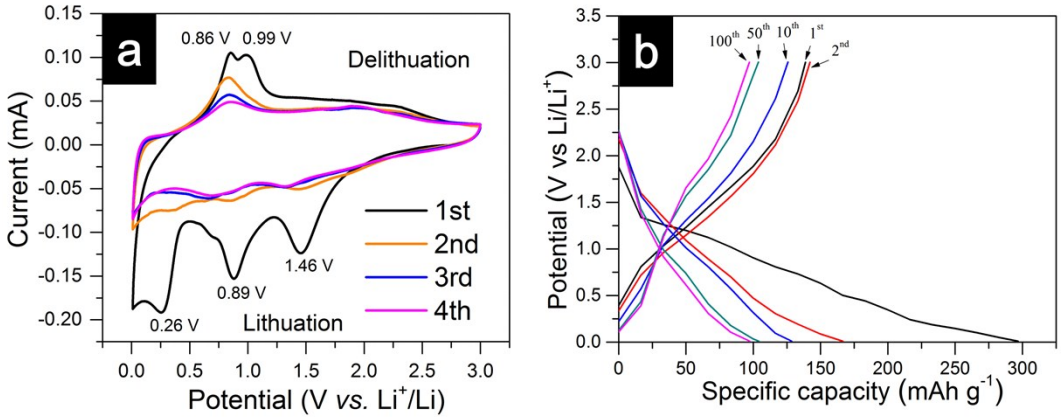

Figure S9. CV (a) and galvanostatic discharge-charge curves (b) of pristine Ti_3C_2.

Table S1. Elements content (at%) by EDS (averaged with 6 data in 20*20 μm of square).

Element	$CNTs@Ti_3C_2$ - Ⅰ	$CNTs@Ti_3C_2$- Ⅱ	$CNTs@Ti_3C_2$- Ⅲ	$CNTs@Ti_3C_2$- Ⅳ	$CNTs@Ti_3C_2$- Ⅴ
C	68.22	75.69	75.91	80.29	85.94
O	16.11	14.24	14.77	11.71	5.92
F	**4.45**	**1.24**	**0.96**	**0.07**	**0.05**
Al	0.34	0.23	0.18	0.10	0.04
Ti	7.29	4.04	3.00	1.95	0.82
Fe	3.60	4.56	5.19	5.88	7.23
Total	100.00	100.00	100.00	100.00	100.00

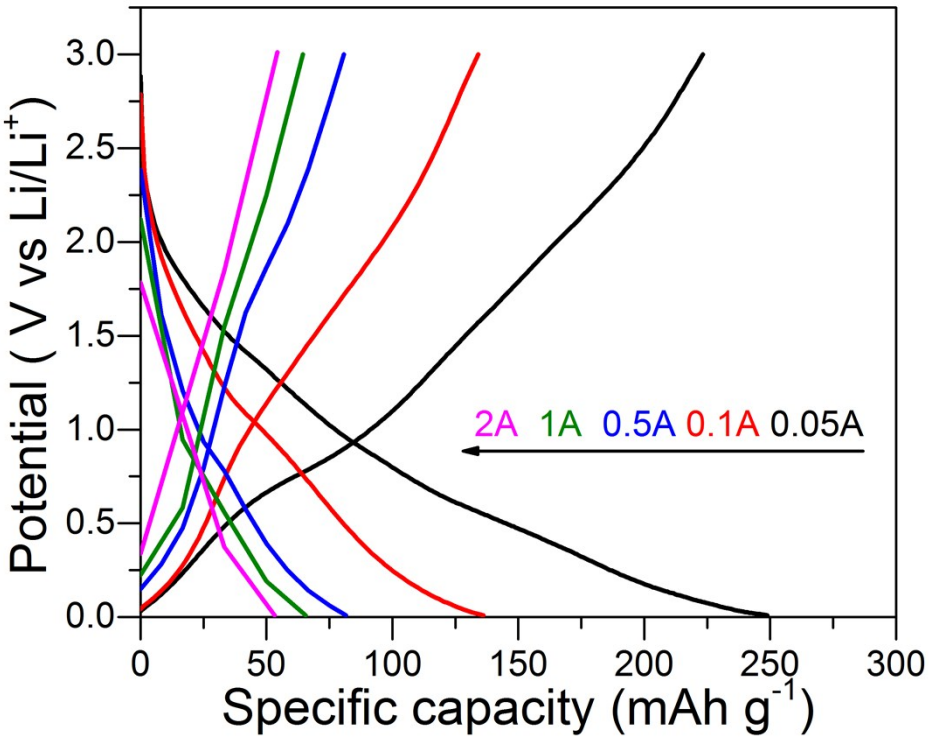

Figure S10. Discharge-charge curves of the pristine Ti_3C_2 at different current densities.

Table S2. Fitting EIS Results of pristine Ti_3C_2 and CNTs@Ti_3C_2-Ⅲ.

Samples	R_s (Ω)	R_{sf+ct} (Ω)	CPE_{sf+ct} (μF)	Z_W ($S \cdot s^{-1/2}$)	C_{int} (mF)	OCP
Ti_3C_2	2.087	50.34	37.05	0.0104	12.34	2.08
CNTs@Ti_3C_2-Ⅲ	2.512	44.32	44.11	0.01989	26.83	2.17

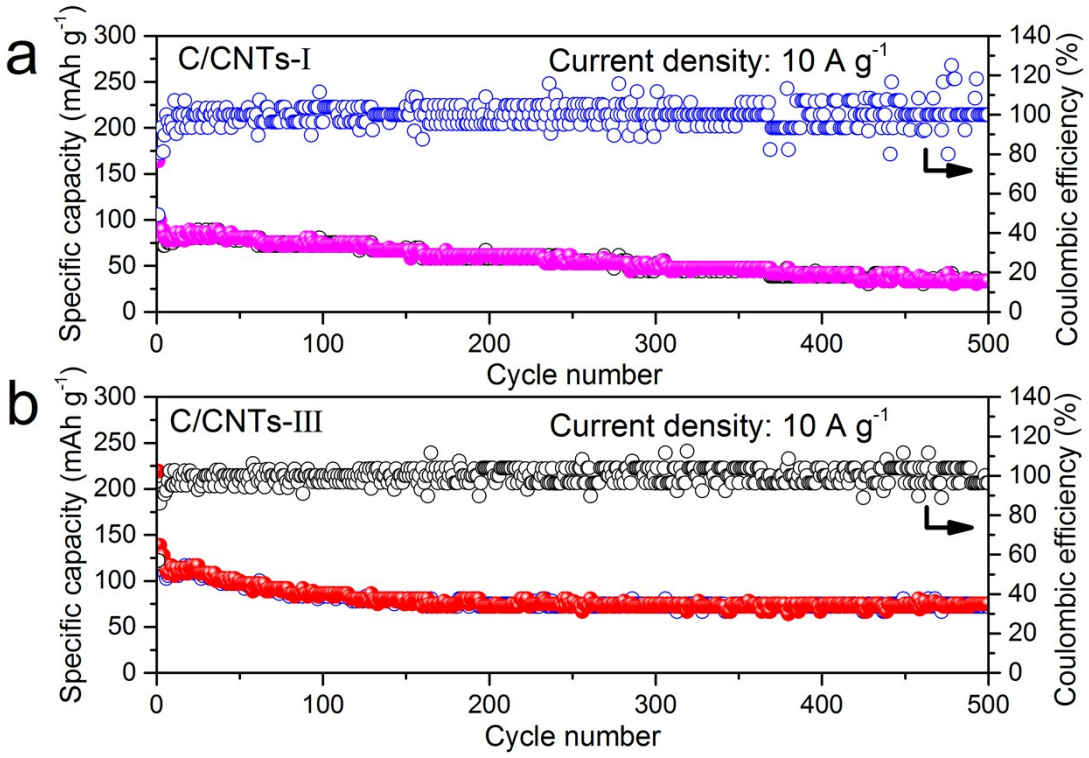

Figure S11. Reversible capacities of C/CNTs-Ⅰ (a) and C/CNTs-Ⅲ (b) at 10 A g^{-1}.

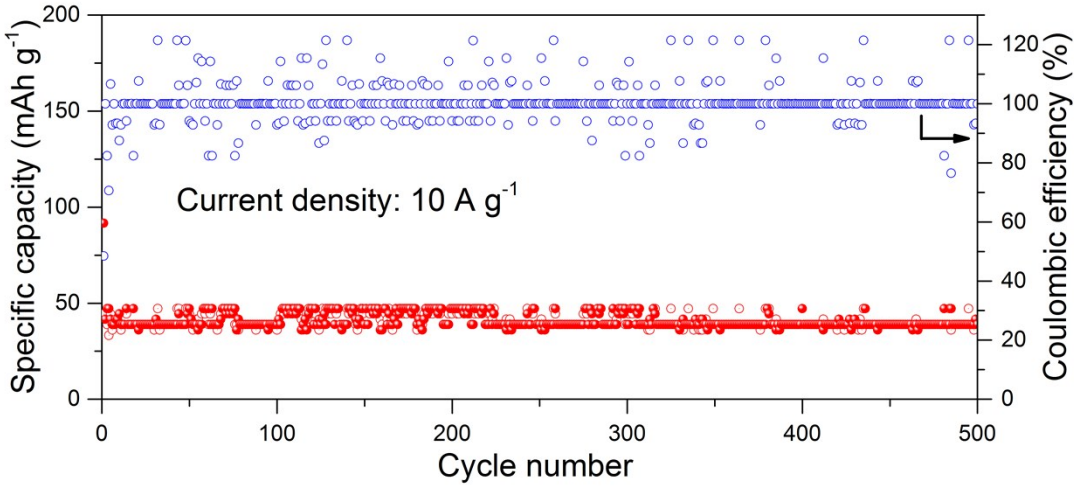

Figure S12. Reversible capacities of Ti_3C_2-Ⅲ at 10 A g^{-1}.

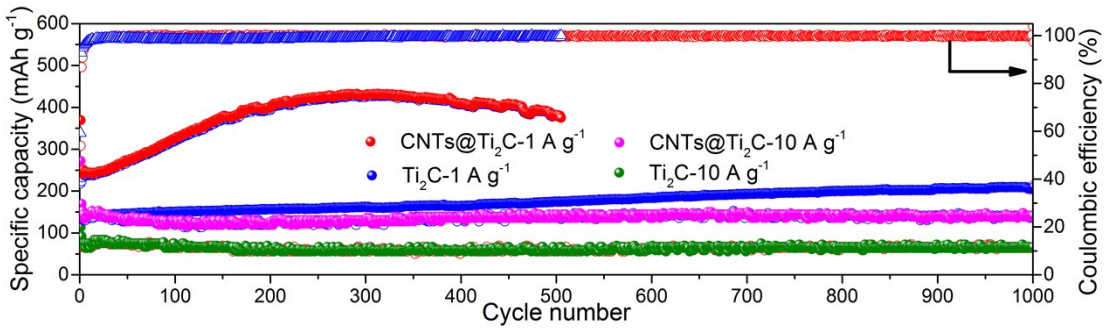

Figure S13. Reversible capacity of Ti_2C and CNTs@Ti_2C electrodes at 1 and 10 A g^{-1}, respectively. Coulombic efficiency is plotted for the Ti_2C and CNTs@Ti_2C electrodes with 1 A g^{-1} only.

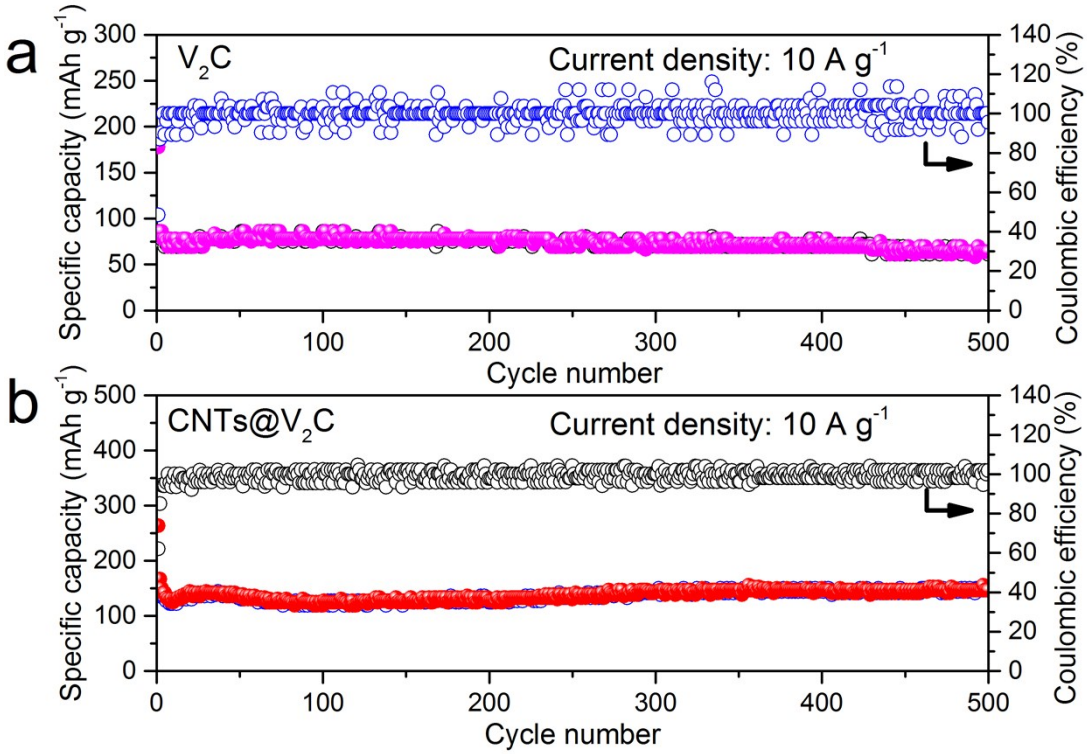

Figure S14. Reversible capacity of V_2C and CNTs@V_2C electrodes at 10 A g^{-1}.